Published in final edited form as:
Brain Topogr. 2013 October ; 26(4): . doi:10.1007/s10548-013-0290-1.

Independent Sources of Spontaneous BOLD Fluctuation Along the Visual Pathway

Jacco A. de Zwart, **Peter van Gelderen**, **Zhongming Liu**, and **Jeff H. Duyn**
Advanced MRI Section, LFMI, NINDS, National Institutes of Health, Bldg. 10, Rm. B1D-728, 9000 Rockville Pike, Bethesda, MD 20892-1065, USA

Abstract

In resting-state functional magnetic resonance imaging (fMRI) experiments, correlation analysis can be used to identify clusters of cortical regions that may be functionally connected. Although such functional connectivity is often assumed to reflect cortico-cortical connections, a potential confound is the contribution of subcortical brain regions, many of which have strong anatomical connectivity to cortical regions and may also enable cortico-cortical interactions through trans-thalamic pathways. To investigate this, we performed resting state fMRI of the human visual system, including cortical regions and subcortical nuclei of the pulvinar and lateral geniculate. Regression analysis was used to investigate the dependence of the measured inter-regional correlations upon afferents from specific retinal, thalamic and cortical regions as well as systemic global signal fluctuation. A high level of interhemispheric correlation (cc = 0.95) was found in the visual cortex that could not be explained by activity in the subcortical nuclei investigated; in addition a relatively low level of inter-hemispheric correlation (cc = 0.39–0.42) was found in vision-related thalamic nuclei that could not be explained by direct anatomical connections or their cortical inputs. These findings suggest that spontaneous fMRI signal correlations within the human visual system originate from a mixture of independent signal sources that may be transmitted through thalamo-cortical, cortico-thalamic, and cortico-cortical connections either trans-callosal or trans-thalamic in origin. Our findings thus call for more cautious interpretation of resting state functional connectivity in terms of any single type of anatomical connectivity.

Keywords

Resting state fMRI; Human visual system; Brain connectivity; Correlation analysis; Callosal pathway; Thalamic pathway

Introduction

Blood oxygen-level dependent (BOLD) functional magnetic resonance imaging (fMRI) experiments are increasingly used to study brain function in absence of overt activity in order to map clusters of functionally related cortical regions. These studies are based on the phenomenon that functionally related cortical regions often show highly correlated spontaneous BOLD signal fluctuations. An example of this is the signal correlation found between homologous functional regions in each cerebral hemisphere, for example bi-lateral sensory-motor cortices (Cordes et al. 2000; Biswal et al. 1995, 1997). Correlated activity between homologous regions in both hemispheres is interpreted to indicate the presence of cortico-cortical connections, a notion that is consistent with the elaborate inter-hemispheric

jacco.dezwart@nih.gov.

connectivity mediated by the corpus callosum. However, it is possible that the inter-hemispheric correlations found in fMRI studies are at least partly caused by subcortical regions that directly or indirectly innervate both hemispheres, without relying on the corpus callosum (Drew et al. 2008). Examples are modulatory process of arousal, selective attention and awareness, whose effect on cortical activity is mediated through subcortical regions (Saalmann and Kastner 2009, 2011; Theyel et al. 2010). Cortico-thalamo-cortical pathways that complement callosal corticocortical pathways have been proposed for such modulatory control (Sherman and Guillery 2011) and in fact have been inferred from analysis of specific cortico-thalamic fMRI resting state correlations (Zhang et al. 2008). Because of its extensive connections with much of the neocortex, the thalamus may mediate many of the cortico-cortical correlations observed in resting state fMRI.

To investigate the contribution of cortico-cortical connections to inter-hemispheric fMRI correlations, several groups have studied brains with abnormal corpus callosum. The results found so far are discordant: in epilepsy patients that underwent surgical transection of much of the corpus callosum, both reduced (Johnston et al. 2008) and largely normal (Uddin et al. 2008) inter-hemispheric fMRI correlations have been found. Similarly, in studies of humans whose brain developed without corpus callosum (acallosal brains), both reduced (Quigley et al. 2003) and normal (Tyszka et al. 2011) inter-hemispheric correlations have been found. In acallosal mice, inter-hemispheric correlations in electrical activity as observed with voltage sensitive dye imaging were found to be much reduced compared to normal mice (Mohajerani et al. 2010). Taken together, these studies suggest that inter-hemispheric cortico-cortical connectivity may not be directly inferred from correlated fluctuations in spontaneous fMRI activity. More generally, a number of studies have indicated the difficulty to interpret cortico-cortical fMRI correlations in terms of direct (mono-synaptic) fiber connections (Damoiseaux and Greicius 2009; Rykhlevskaia et al. 2008; Adachi et al. 2012).

To further study this issue, and assess the contribution of subcortical input to inter-hemispheric cortico-cortical correlations, we preformed fMRI experiments of the visual system in normal human subjects. This system was chosen as its anatomical and functional substrates are relatively well established, and it has a large cortical representation that generally shows robust spontaneous activity. Spontaneous fMRI signals were extracted from bilateral visual cortices (VIS), the subcortical (thalamic) bilateral lateral geniculate nuclei (LGN), and several other deep brain nuclei such as the bilateral nuclei of the pulvinar (PUL), after which correlation analysis was performed to establish potential contributors to cortical activity.

Materials and Methods

Background

As can be observed from a schematic summarizing the major processing nodes in early visual processing (Fig. 1), there are several subcortical regions that can exert strong influence on activity in VIS (Van Essen et al. 1982; Saalmann and Kastner 2011; Sherman and Guillery 2006). During natural vision, the largest and retinotopically most specific part of visual information received with the eyes is processed along a primary pathway through the LGN to VIS sub-regions V1 and MT, and from these regions onto high order visual areas. A secondary pathway of information flow to V1 runs through PUL, either directly or indirectly through the superior colliculi (SC). PUL also has extensive bidirectional connections with VIS. Both these primary and secondary pathways receive modulatory control from various brain stem nuclei, including those from the so-called ascending reticular activating system (ARAS) (Moruzzi and Magoun 1949).

The often strong inter-hemispheric correlation observed between bilateral VIS may originate from a number of sources, and may reflect inter-hemispheric connections between cortical as well as between subcortical regions. For example, there are extensive callosal connections between most sub-regions of VIS, with the notable exception of bilateral V1, between which anatomical connections are sparse. In contrast, the subcortical LGN and PUL have no known direct inter-hemispheric connections, but they both receive extensive modulatory input from ARAS and/or SC, regions that have either direct or indirect inter-hemispheric connections.

In order to distinguish between subcortical and cortical contributions to the inter-hemispheric functional connectivity that has been observed in VIS, one would ideally want to monitor spontaneous activity in all major nodes of the visual pathway as indicated in Fig. 1. Unfortunately, for various reasons, fMRI activity in retina, SC and ARAS has proven difficult to measure (albeit SC fMRI has been previously demonstrated (Schneider and Kastner 2005)). With this in mind, we focused our study on VIS, LGN, and PUL. (An atlas-based SC ROI was included, as will be explained below, but could not be specifically targeted to the most relevant SC-layers). Since the influence of retina, SC, and ARAS on activity in VIS is effectuated through LGN and PUL, this limitation was not expected to affect our primary aim of investigating subcortical effects on cortico-cortical connectivity.

MRI Experiments

MRI experiments were conducted on healthy human volunteers (7 male, 6 female, average age 36.4 ± 10.5 years), all of which provided informed consent as part of an institutional review board approved protocol. The experiments were performed on a General Electric (Milwaukee, WI, USA) Signa 7 T scanner equipped with a 32-channel receive-coil array (Nova Medical, Wilmington, MA, USA) and head transmit coil (Nova Medical). Each experiment included a 12-min fMRI scan to functionally localize cortical and subcortical visual regions (first 5 min), and to record spontaneous activity in these regions (2 min of eyes-open (EO) rest and 5 min of eyes-closed (EC) rest), and a separate anatomical scan to further localize the LGN.

The localizer paradigm consisted of a 30/30 s on/off, 7.5 Hz full-field checkerboard task and was used to identify left and right LGN as well as visual cortex (Chen et al. 1998). During localizer and EO rest, volunteers were instructed to focus on a dot in the center of the image, which alternated in color between red and pink at a randomly varying interval of between 4 and 16 s. Volunteers were instructed to press a button on an MR compatible button box (fORP, Current Designs, Philadelphia, PA, USA) to mark the timing of the color changes. Button presses, as well as MR slice timing triggers, were recorded using Presentation software (Neurobehavioral Systems, Albany, CA, USA), which was also used to present the stimulus images. A message briefly displayed on the screen 7 min into the experiment, at the end of EO rest, prompted volunteers to close their eyes for the last 5 min of the scan, after which the screen turned black. Only the block-paradigm task and EC-rest periods of the data were analyzed for this study. The fMRI experiment used a gradient-echo echo-planar imaging (EPI) technique with the following parameters: $2.5 \times 2.5 \times 2.0\ mm^3$ voxels; 30 ms echo time (TE); 2 s repetition time (TR); twenty 2-mm axial slices with 1 mm inter-slice gap; rate-2 sensitivity encoding (SENSE) (Pruessmann et al. 1999); $240 \times 180\ mm^2$ field-of-view (FOV); 90° nominal flip angle; 250 kHz acquisition bandwidth; ramp sampling on approximately 50 % of the ramps (ramp duration is 164 μs). The echo train length and spacing were 21.7 ms and 592 μs, respectively.

High-resolution anatomical data were acquired as well to aid in selection of bilateral LGN regions of interest (ROIs). For this purpose, dual-echo susceptibility weighted gradient echo data were acquired with scan parameters: rate-3 SENSE acceleration, 1024 × 256 acquisition

matrix size (1024 × 768 following SENSE reconstruction), 0.23 × 0.23 × 1.0 mm^3 resolution, 39 slices, 0.5 mm inter-slice gap, 240 × 180 mm^2 FOV, 15.0 and 34.3 ms TE, 1200 ms TR, 60-degree nominal flip angle. Slices were positioned such that every other slice in the high-resolution data coincided with a slice in the fMRI data. Fully-sampled lower-resolution data (128 × 96 matrix size; 1.9 × 1.9 mm^2 in-plane resolution) were acquired in the same slice locations to serve as coil-sensitivity data for use in the SENSE reconstruction of the high-resolution data. To keep scan time of this coil sensitivity scan short (~1 min) a 6-ms TE was used in combination with 550-ms TR and a 45-degree nominal flip angle. An example of high-resolution anatomical data for the first echo is shown in Fig. 2.

Cardiac and respiratory traces were recorded using the pulse oximeter and respiratory bellows, respectively, which were part of the MRI system. These signals, recorded at 250 Hz, were used for physiological noise regression during data analysis. For synchronization, MR timing in the form of one TTL trigger per acquired volume was recorded using the same software. For respiration, the actual waveform was available, whereas for the cardiac cycle only the heart beat timing was available in the form of TTL pulses.

Data Analysis

Five volunteers were excluded because they either performed the attention task poorly, or because the localizer block paradigm scan failed to identify significantly activated voxels in either left or right LGN. The remaining eight volunteers (five male, three female, average age 36.4 ± 7.6 years) demonstrated continued attention to the task, as indicated by a correct button press ratio of 0.94 ± 0.03 (mean ± standard error), accounting for both missed color changes as well as erroneous button presses. The worst performer showed a 0.81 ratio. One volunteer had misunderstood the task and only pressed the button for color changes from red to pink, not from pink to red. The resulting ‘missed’ button presses were not counted as erroneous in that particular case.

After image registration, the functional localizer data were analyzed using a conventional general linear model (GLM) analysis, assuming a hemodynamic response function (HRF) with a latency and full-width at half maximum (FWHM) of 3.5 s each. Four trend regressors (zeroth through third order) were also included in the design matrix to account for slow signal drifts. LGN ROIs were manually selected in the resulting activation maps using the high-resolution gradient-echo data as an anatomical reference. All significantly activated voxels that anatomically corresponded to the left and right LGN were included in the left and right LGN mask, respectively. As expected, the LGN activation typically appeared as two clearly distinct, contiguous bilateral areas (e.g. see Fig. 2). All significantly activated voxels that were not part of LGN were assigned to the visual cortex ROI (referred to as VIS), which was subsequently split along brain midline after a 3-voxel wide strip encompassing the midline was discarded. The resulting two ROIs are referred to as VIS_L and VIS_R hereafter.

Before cross-correlation (CC) of the signal in LGN and VIS ROIs was carried out, multi-regression analysis was performed to remove several nuisance signals related to both the time of acquisition with respect to cardiac and respiratory events (= phase) as well as changes in the period of the cardiac and respiratory cycle (= rate). For this purpose, four cardiac and respiratory phase regressors were derived using RETROICOR (Glover et al. 2000), using two harmonics for both cardiac and respiratory signals. Two cardiac rate regressors with lag −3 and +9 s (Shmueli et al. 2007), and two respiratory rate regressors with lags −9 and +9 s, derived in similar fashion as was described in (Birn et al. 2006), were also regressed out.

The initial analysis focused on the primary visual pathway (retina → LGN → VIS). CC of ROI-averaged time series signals was performed on the resulting filtered data, both for the eyes-closed rest period and the data acquired during the block-paradigm checkerboard task. The block paradigm data were included in the analysis to investigate to what extent the findings were affected by coherent signal input to the retina, which subsequently yields coherent signals in both hemispheres without the need for callosal synchronization.

Note that for each area only the overall temporal signal fluctuation is known, which may contain contributions of several independent signals, such as: a fluctuation shared with another area; an independent signal only found locally; and random noise. The presence of these independent signals as well as their relative contribution to the signal in each ROI is unknown, since they cannot be assessed independently using resting-state BOLD fMRI. To further investigate the possible source of the signal coherences thus established, regression was employed to remove the mean signal in one area from the voxel time courses in other areas, and to investigate the effect of this removal on the various cross correlation values. This is a basic form of partial correlation analysis (Whittaker 1990), which can shed light on the presence and relative importance of common signal fluctuations, thus aiding in understanding the observations.

Several of these regression-based signal removal strategies were employed here. First, we evaluated how the correlation between bilateral LGN depended upon their respective cortical (feedback) afferents from the visual cortex. The ROI-averaged visual cortex signal in each hemisphere was removed from the individual signal time courses in the voxels in the corresponding LGN ROI. (The mean signal in VIS_L was regressed out from the voxels in LGN_L, and the mean from VIS_R was regressed out from the LGN_R voxels). After this regression step the cross correlation analysis was repeated. Similarly, we also evaluated how the correlation between bilateral VIS depended on their subcortical (feedforward) afferents from LGN. The mean LGN signal time course for each hemisphere was removed from the visual cortex voxels in the same hemisphere before cross correlation analysis was performed. This was done for both the eyes-closed resting state and task data.

The task data were included in the investigation to examine the effect of retinal input on the observed interregional correlations. Assessing the task-independent interregional coherences requires removal of the task-related response. Therefore, on the visual task data, one of the following three additional regression-based removal strategies was performed in order to discount stimulus-driven retinal inputs in the correlations between cortical and subcortical areas:

- The modeled response to the block paradigm was removed from the data (this is the same regressor that was used to detect activation, see above) before regression analysis was performed.

- The mean time course signal in the visual cortex was computed. It was separated in five sections, each corresponding to a 1-min period centered around one ‘on’ block. These five 30-sample sections were subsequently averaged and the result replicated five times to yield a regressor describing the mean response to the five task ‘on’ blocks (see Fig. 3). Regression analysis was performed after removal of this mean response time course.

- The equivalent of this procedure was performed using the mean time course signal in LGN instead of the visual cortex, yielding a mean LGN response time course.

Monte Carlo Simulation

In order to provide more insight into the source of the observed correlation between the bilateral Lateral Geniculate Nuclei, independent source signals were generated for a Monte Carlo simulation and combined with various amplitudes to represent the observed fMRI signals (S) in LGN and VIS regions. This was done to establish the ranges of the relative contributions of these independent signals that yield experimentally observed correlation values. To this extent, the following five independent signals (I) were generated:

I_{all}—A signal common to both the visual cortex and LGN, in both hemispheres, I_{vis}—A signal found only inside the visual cortex (in both hemispheres), $I_{lgn,com}$—A signal found in both left and right LGN but not in visual cortex, $I_{lgn,latL}$—A signal present only in the left LGN, $I_{lgn,latR}$—A signal present only in the right LGN.

These five signals were all assumed to have the characteristics of normally distributed noise. Using combinations of these five unique signals, simulated resting state signals for the visual cortex, the left LGN and the right LGN were derived. The above source signals were multiplied with amplitudes (a) that were iteratively adjusted:

$$S_{vis}=a_{\mathrm{all}} * I_{all}+a_{\mathrm{vis}} * I_{vis}$$

$$\mathrm{S}_{\mathrm{lgnL}}=a_{\mathrm{all}} * \mathrm{I}_{\mathrm{all}}+a_{\mathrm{lgn,com}} * \mathrm{I}_{\mathrm{lgn,com}}+a_{\mathrm{lgn,lat}} * \mathrm{I}_{\mathrm{lgn,latL}}$$

$$\mathrm{S}_{\mathrm{lgnR}}=a_{\mathrm{all}} * \mathrm{I}_{\mathrm{all}}+a_{\mathrm{lgn,com}} * \mathrm{I}_{\mathrm{lgn,com}}+a_{\mathrm{lgn,lat}} * \mathrm{I}_{\mathrm{lgn,latR}}$$

Source amplitudes a_{all}, a_{vis}, $a_{lgn,com}$ and $a_{lgn,lat}$ were each independently modified in a stepwise fashion in the Monte Carlo simulation. Note that the left and right visual cortex where not separately simulated, since in the experimental data they were found to be highly correlated (CC ~ 0.95, see “Results” section, below), and therefore they were assumed to be identical in this simulation. Similar to what was done when analyzing the experimental data, the VIS signal (S_{vis}) was regressed out of both S_{lgnL} and S_{lgnR}, yielding two additional signals referred to as $S_{lgnL,filt}$ and $S_{lgnR,filt}$. Four cross correlation values were computed from these different data sets, namely: CC(S_{vis}, S_{lgnL}), CC(S_{lgnL}, S_{lgnR}), CC(S_{vis}, $S_{lgnL,filt}$) and CC($S_{lgnL,filt}$, $S_{lgnR,filt}$). Since S_{lgnL} and S_{lgnR} behave similarly (albeit without being identical), corresponding values such as CC(S_{vis}, $LGN_{R,filt}$) were not computed. For the same reason the term S_{lgn} is used below, which is meant to represent either S_{lgnL} or S_{lgnR}.

In this simulation, the amplitudes of all four independent source signals (a_{all}, a_{vis}, $a_{lgn,com}$ and $a_{lgn,lat}$) were separately changed in 64 steps (ranging linearly from 0 to 63), and random signals were repeatedly (256 repeats) calculated for each set of amplitude indices and each independent source (I_{all}, I_{vis}, $I_{lgn,com}$, $I_{lgn,latL}$ and $I_{lgn,latR}$). Each signal consisted of 150 time points, similar to the number of time points acquired during the eyes-closed resting state period in the actual fMRI experiments. After calculating the combined signals in each region, correlations between all node pairs were calculated and averaged across the 256 repeats. Simulated and experimentally determined cross correlation values were compared and considered consistent if they were within one standard error as determined from the experimental data (see Table 1).

Selection of Reference Regions and ROIs for Relevant Deep-Brain Nuclei

To investigate whether the observed cross correlations may have been caused by some non-specific (e.g. systemic) signal fluctuation instead of signals specific to the visual system, the analysis was repeated using comparable thalamic and cortical areas that were not part of the visual system. An arbitrarily-picked thalamic area near LGN (and outside other possibly relevant thalamic nuclei, such as the PUL) was selected in each hemisphere, approximately located in the ventral medial nucleus. In addition, bilateral insular cortex was selected to serve as a cortical reference, because of its independence of visual cortex.

The thalamic reference area was selected with aid of a stereotactic atlas of the human thalamus (Morel 2007) as follows: The location of the center of gravity (COG) of the LGN nucleus in the atlas was determined, as well as the COG for the thalamic reference area. The displacement vector (in mm) for these two atlas-based ROI-COGs was then computed. Independently for each hemisphere, the COG of the LGN in EPI data space was determined based on the LGN activation ROI derived from experimental data. This LGN-COG was subsequently used, in combination with the atlas-derived displacement vector, to determine the center of a 3 × 3 × 3-voxel ROI in the MR data. This is to ensure that even if artifacts, such as geometrical distortions due to B_0 inhomogeneities, or anatomical inter-individual differences, caused the thalamus as a whole to be in a somewhat different location, the ROI would still correctly represent the nucleus as long as the thalamus size and shape did not vary drastically. This is plausible since the various thalamic nuclei of interest are in close proximity of each other and EPI distortions in the thalamus were found to be on a sub-voxel level (data not shown).

The insula area was selected in the following manner. First, the insular cortex in both hemispheres was manually outlined in three of the imaging slices, using both an atlas of the human brain (Duvernoy 1999) and the anatomical scan for the same volunteer as a guide. For each hemisphere independently, the mean signal during eyes-closed rest within the ROI for that hemisphere was computed. The correlation between this mean and the time course of each individual voxel in the ROI for that hemisphere was then computed. Voxels that yielded a correlation greater than or equal to 0.5 were used to define the insula ROI for that hemisphere.

In addition to the brain areas along the primary visual pathway (LGN and VIS), other deep-brain nuclei are known to be involved in vision. Since task-based selection of those nuclei was not feasible, the method employed to derive the thalamic reference ROI was used. In that fashion, bilateral ROIs of 3 × 3 × 3 voxels per hemisphere were also selected for PUL and SC, as well as for the anteriodorsal and mediodorsal thalamic nuclei, which play a role in attention and alertness modulation. Note that SC is rather small (Schneider and Kastner 2005), so that the SC ROI risks including some signal from neighboring tissue. However, since our atlas-based localization might be imprecise, the larger ROI allowed for a 1-voxel tolerance in each direction.

Finally, a global mean signal regressor mask was obtained by selecting the entire brain (defined as all voxels in which the signal exceeded 3 % of the maximum signal in the 10th imaging volume) and excluding from it the voxels that were in any of the ROIs described earlier.

Results

Localization of LGN and Visual Cortex

Figure 2 shows an example of LGN and visual cortex activation obtained from the block paradigm experiment, superimposed on the high-resolution anatomical gradient echo image.

The number of activated voxels in LGN for the eight volunteers that were included in data analysis is 7.3 ± 1.8 for LGN_L and 7.8 ± 1.7 for LGN_R, (mean ± standard error over volunteers). Sizes of the visual cortex ROIs were 804 ± 163 and 801 ± 225 for VIS_L and VIS_R, respectively. Insular ROIs were respectively 157 ± 29 and 144 ± 23 voxels in size.

Cross Correlation Analysis During Eyes-Closed Rest

Cross correlation analysis of spontaneous activity during the rest period showed that significant correlation between left and right LGN (0.39 ± 0.07) (mean ± standard error over volunteers, Table 1), despite the absence of a direct callosal connection. The significance thresholds ($p < 0.05$) for the reported correlation values are 0.17 and 0.21 without and with a correction for multiple (8) comparisons, respectively. Correlation between left and right visual cortex was consistently found to be very high (0.95 ± 0.01). Regression-based exclusion of the mean visual cortex signal from LGN voxel time courses for the same hemisphere shows persistence of the correlation between left and right LGN, as can be seen in Table 1. This table also shows the results of cross correlation analyses following the other regression strategies for both eyes-closed rest and task data. Importantly, the results suggest a correlation between left and right LGN not caused by feedback from the visual cortex.

This finding was further confirmed by partial correlation analysis (e.g. (Salvador et al. 2005)), where the correlation between each pair of areas of interest is corrected for the contribution of all other areas of interest. This partial correlation analysis was performed on the basis of the mean resting state signal in each hemisphere in the eight areas investigated, yielding a total of 16 source signals, see Fig. 4. The partial correlation for LGN_L–LGN_R was found to be 0.30 ± 0.05, and 0.29 ± 0.05 after global signal regression. This further demonstrates that a significant interhemispheric correlation between LGNs exists, which cannot be simply attributed to any of the areas taken into account, or by non-specific global signal fluctuations.

Similarly, regression-based removal of LGN did not eliminate the correlation between VIS_L and VIS_R, indicating that LGN resting state fluctuations are not fully synchronized with visual cortex fluctuations and vice versa. Persistence of the interhemispheric LGN correlation indicates that the lower level of correlation between LGN_L and LGN_R, when compared to the strong VIS_L–VIS_R correlation, is not merely the result of reduced image SNR (increased intrinsic noise level) in LGN, or a partial volume effect yielding reduced cross correlation between left and right LGN. This is supported by the amplitude of the fluctuations in both LGN and visual cortex, which exceed the intrinsic (thermal) noise level by at least a factor of two (Table 2).

Monte Carlo Simulations of Causality

Results of Monte Carlo simulations were searched to find conditions (combinations of signal amplitudes a_{all}, a_{vis}, $a_{lgn,com}$ and $a_{lgn,lat}$) that yielded cross correlation values which matched the experimental findings within a range of one standard error (as was reported in Table 1). The amplitude of S_{lgn} relative to S_{vis} served as an additional exclusion criterion, since the measured fluctuation levels in LGN and VIS were similar (see Table 2). Since measured LGN/VIS fluctuation level ratio was 0.93 ± 0.40 (mean ± standard deviation over the 8 volunteers), it was decided that S_{vis} and S_{lgn} amplitudes that deviate by more than a factor of 2 were not realistic. Therefore only combinations yielding S_{vis} and S_{lgn} amplitudes in this range ($0.5 \leq S_{lgn}/S_{vis} \leq 2.0$) were selected.

A total of 169126 conditions matched all criteria, constituting 1.01 % of the total number of simulated conditions. The component signal amplitudes (a), all scaled relative to S_{lgn}, for these matching conditions are shown in Fig. 5. Results indicate that the finding of persistent

correlation between left and right LGN, independent of removal of the visual cortex signal using regression, does not require a bilateral LGN signal independent from visual cortex ($a_{lgn,com}$, the x-axis in Fig. 5). This because valid sets of [a_{all}, a_{vis}, $a_{lgn,com}$, $a_{lgn,lat}$] exist where $a_{lgn,com}$ is zero, as is shown in Fig. 5. Furthermore, the simulations suggest the simultaneous presence of a bilateral source signal in visual cortex that is not present in LGN (a_{vis}, the green curve in Fig. 5), lateralized signals originating in the LGN (or upstream areas) ($I_{lgn,lat}$, the black curve in Fig. 5) and a (somewhat smaller) source signal common to all nodes investigated (aall, the blue curve in Fig. 5). This is demonstrated by the fact that a_{all}, a_{vis} and $a_{lgn,lat}$ for the results shown in Fig. 5 are all distinctly non-zero. Simulations with one or more of these amplitudes close to and at zero were performed (see "Materials and Methods" section), but none of these yielded a valid match that could explain the experimental data.

Cross Correlation Analysis During Task

Cross correlation analysis on the task-phase of the data shows that independent signals are present in that brain state as well (Table 1). Removal of VIS signal from LGN voxels, or LGN signal from VIS voxels, for the corresponding hemisphere does lead to a reduced interhemispheric cross correlation in those regions, but the remaining cross correlation is still significantly larger than zero. Note that removal of the paradigm regressor (block paradigm convolved with HRF, see "Materials and Methods" section) yields a smaller decrease in cross correlation in both LGN and VIS than removal of the mean VIS or LGN time courses, further evidence that signal fluctuations not directly related to the task are simultaneously present in both areas. To demonstrate that this finding is not merely a result of an incorrect HRF model, the average response to an event block (mean over the five task 'on' blocks of the ROI-averaged response, see Fig. 3) in LGN or VIS was also used as a regressor. Use of this block-averaged regressor also yields a diminished cross correlation decrease compared to when the ROI-averaged response itself was used, again demonstrating that signal fluctuations that are not related to the block-paradigm task, but are common to both LGN and VIS, are present during this experimental phase.

The level of signal fluctuation was only marginally higher during task than rest, namely 1.5 ± 0.6 % of baseline signal (task) versus 1.1 ± 0.1 % (rest) in VIS, and 1.3 ± 0.3 % versus 0.9 ± 0.1 % in LGN, respectively, all on an ROI level. After regression-based paradigm removal, residual fluctuation level decreases to 1.0 ± 0.3 % in LGN and 0.9 ± 0.3 % in VIS, not significantly different from the fluctuation level during the rest-phase of the experiment. Removal of the mean VIS signal (instead of the HRF-convolved paradigm) from LGN led to a residual fluctuation level of 0.9 ± 0.3 % in LGN, whereas removal of the mean LGN signal from VIS resulted in a fluctuation level of 1.1 ± 0.3 in VIS.

Contribution of Systemic Fluctuations

To investigate contribution of systemic fluctuations to the above findings, cross correlation analysis was repeated after regression-based removal of the global mean signal. The global mean signal regressor was defined as the mean signal time course in most of the brain, excluding only the voxels that were a member of any of the ROIs used. The correlation analysis was also performed using the reference thalamic and insula ROIs, as well as the other nuclei of interest, and compared to the CC data obtained when global mean signal was not removed. Results of these analyses are shown in Table 3.

It was found that significant correlation with visual cortex and LGN exists for most of the other regions investigated, including both the thalamic reference region and insula, if global signal regression (GSR) is not performed. However, GSR reduces these correlations substantially, resulting in non-significant correlation with LGN and VIS for several of the

areas investigated. However, global signal regression leads to only a minor reduction in the cross correlation between LGN and visual system, and the inter-hemispheric correlation of all regions investigated (including the reference regions unrelated to the visual system) is also retained following GSR. Note that some CC values become negative following GSR (albeit without reaching statistical significance), suggesting some degree of over-correction, where some signal of interest is also removed by GSR. This post-GSR analysis demonstrates that while some global signal fluctuation is present in these data, it is not the source of the findings presented above. This indicates that the fluctuations observed in the visual system are predominantly functionally specific, a notion supported by the observation that unlike other thalamic nuclei, the correlation of both PUL and LGN with VIS does not become negative following GSR. This distinction between PUL and LGN, with known involvement in vision, on one hand and other thalamic nuclei on the other also implies that visual cortex signal coherence with LGN does not involve all of thalamus. The consistently negative CC between thalamus and VIS described previously (Zou et al. 2009) was not observed here.

The somewhat diminished cross correlation values found after global signal regression do not alter the conclusions drawn from Monte Carlo simulations, as a comparable set of simulated source amplitude distributions matched these post-GSR experimental data (results not shown).

Table 2 shows the fluctuation level in the various regions of interest before and after GSR, both at the voxel level and the ROI level during the EC resting state phase of the experiment. The image (intrinsic) noise level (derived from the inverse of the image SNR) is also shown. The reduction in fluctuation level is minimal when global signal is removed, further evidence that such global fluctuations are not the dominant source of signal coherence in any of the areas investigated. Furthermore, the signal fluctuation level is at least two times larger than the intrinsic noise level in all areas.

Discussion

In the present work, the coherence of resting state signal fluctuations between components of the human visual system was investigated, with a focus on LGN and the visual cortex. Strong bilateral correlations were found in VIS, consistent with earlier reports (Lowe et al. 1998). It was also found that left and right LGN show strong inter-hemispheric correlation, despite the absence of a direct neuronal connection. Furthermore, intra-hemispheric resting state correlation between LGN and visual cortex was relatively low, and regression-based removal of LGN signal from visual cortex, and vice versa, showed that fluctuations in either one of these areas does not solely reflect (a component of) the fluctuation present in the other area. In addition, correlated bilateral fluctuations in PUL and other thalamic brain areas directly or indirectly involved in modulatory control of visual throughput to the visual cortex are too weak to explain the observed inter-hemispheric VIS correlation. Therefore, this inter-hemispheric cortico-cortical correlation found in VIS appears to reflect cortico-cortical connectivity. The computed partial correlation matrix and results of Monte Carlo simulations support these findings, showing that the source of the inter-hemispheric correlation in LGN is ambiguous and may either lie in the visual cortex or upstream/modulatory areas such as retina and brainstem (Worgotter et al. 2002). Specifically, the low but significant inter-hemispheric correlation in LGN and PUL may arise from cortical feedback or be the result of subcortical effects in upstream areas mediated by ARAS and SC. Subcortical sources may include the parabigeminal and parabrachial nucleus of the Pons, as well as the thalamic reticular nucleus. (A recent study showed the effect of focal pontine lesions on functional connectivity (Lu et al. 2011), providing evidence of the contribution of poly-synaptic pathways to functional connectivity.) There also may be inter-hemispheric correlation introduced by bilateral eye movement mediated by SC. As was

pointed out above, the analysis indicated that the strong inter-hemispheric VIS correlation cannot be explained by correlated input from LGN or PUL, suggesting that the strong inter-hemispheric correlation in VIS reflects cortico-cortical connectivity. Such connectivity is mostly absent for area V1, with the exception of areas representing the vertical meridian of the visual field, along the V1/ V2 border, but substantial callosal connections exist for higher visual areas in primates (Van Essen et al. 1982; Clarke and Miklossy 1990), including humans.

Since the individual signals that contribute to the various areas cannot be adequately separated using fMRI (or other non-invasive neuroimaging techniques, such as Magnetoencephalography, MEG, or Electroencephalography, EEG), but only inferred, and since BOLD fMRI of the retina is challenging, it may not be possible to reveal the precise origins of these signals with fMRI. Presumably more invasive electrophysiological experiments in animals would be required to reveal all contributors to the observed fMRI correlations with certainty. One such study has recently shown the presence of two distinct neural activity patterns in supra- and infra-granular VC layers during both rest and stimulation (Maier et al. 2010), demonstrating the presence of multiple potential contributors to fMRI correlations within VIS. A recent study has also shown layer specific fMRI response and correlation patterns in VIS (Polimeni et al. 2010).

This layer-specific phenomenon may explain the relatively low bilateral LGN correlation in the presence of strong bilateral VC correlation found in the current study. Specifically, bilateral VC correlation may reflect activity in supra-granular layers, which may not effectively transfer to the LGN through the infra-granular layers, which appear functionally distinct (Fig. 6). It would also explain why regression of VIS signal from LGN fails to reduce bilateral correlation in LGN. If a substantial contributor to the overall VIS signal is not fed back to LGN, the overall VIS signal does not correctly describe a component of the LGN signal, and removal of the VIS contribution from LGN will be reduced.

Noise analysis showed that the low level of bilateral correlation in LGN, relative to that in VC, is not simply the result of lower SNR (increased intrinsic noise level) in LGN, or the reduced averaging due to the smaller number of voxels. The low contrast to noise level combined with the small number of voxels in LGN might lead to a minor underestimation of the correlation values (de Zwart et al. 2013), but correcting for this effect (See “Appendix”) would only yield a minor increase in $CC(LGN_L, LGN_R)$ to 0.44 ± 0.08 (from 0.39 ± 0.07, see Table 1). Note that $CC(LGN_L, LGN_R)$ is the value most affected by this effect due to both left and right LGN ROIs being small, the effect of intrinsic noise on other correlation values is notably smaller. The lower bilateral LGN correlation when compared to VIS may therefore be an indication of a lower connection strength through direct or indirect synaptic pathways (Honey et al. 2009). However, this cannot be concluded based on the current set of data and analysis approaches, which did not allows us to unequivocally establish the origin(s) of the inter-hemispheric LGN–LGN correlation.

Another potential confound that could affect this kind of inter-regional correlation analysis is differences in HRF between the various areas involved. Significant differences in HRF could lead to different degrees of filtering of the neuronal signals underlying the measured BOLD-fluctuation time courses. This is not inconceivable, since we have previously shown that even within a cortical brain area there are notable differences in HRF (de Zwart et al. 2009; de Zwart et al. 2005). We assessed the extent to which this contributed to our findings by re-analyzing the data following low-pass filtering (≤0.1 Hz), which would suppress the effects of such HRF differences. No substantial differences in correlation values were found, suggesting the findings did not originate from regional differences in HRF.

In summary, correlated spontaneous activity exists between all visual system nodes studied, including those without monosynaptic connections. Correlations between bilateral LGN did not entirely arise from bilateral visual cortex activity or vice versa, suggesting that other pathways contribute to these. Potential contributors are other nodes of the visual pathway, either upstream or downstream from the areas studied. These findings demonstrate that inter-hemispheric correlations may be observed in various brain areas that do not have direct callosal connections; such correlations may be supported by multi-synaptic pathways that do not necessarily involve corpus callosum and that may be transmitted through thalamo-cortical, cortico-thalamic, and cortico-cortical connections. It thus calls for more cautious interpretation of resting state functional connectivity in terms of any single type of anatomical connectivity.

Acknowledgments

This work was sponsored by the Intramural Research Program of the National Institute of Neurological Disorders and Stroke, NIH.

Appendix

Correction of Attenuation of Correlation

(This Appendix is based on (de Zwart et al. 2013).)

It is well established that noise sources may attenuate the temporal correlation between signals, an effect first described in (Spearman 1904). This effect, known as attenuation of correlation, may be important for the interpretation of resting state fMRI, where non-neurogenic noise sources coexist with signals of interest. We propose a procedure for determining functionally relevant CC based on estimates of the amplitude of thermal noise. The level of random (thermal) noise in regions *a* and *b* of the image can be estimated from a zero-flip angle measurement. Based on this, the noise-corrected CC between two time series measurements (i.e. signal + noise) u_a and u_b in regions *a* and *b* can be calculated as follows:

$$CC_{corrected}=CC_{observed}\cdot\sqrt{\left(\frac{\mathrm{var}\,(u_a)\cdot\mathrm{var}\,(u_b)}{(\mathrm{var}\,(u_a)-\mathrm{var}\,(n_a))\cdot(\mathrm{var}\,(u_b)-\mathrm{var}\,(n_b))}\right)} \quad (1)$$

where var(·) is the variance in the time-series signal or noise measurement (*n*). It should be noted that this correction does not improve significance of the result but merely improves accuracy of the estimated CC, e.g. allowing for CC comparisons between areas suffering from different levels of thermal noise.

References

Adachi Y, Osada T, Sporns O, Watanabe T, Matsui T, Miyamoto K, Miyashita Y. Functional connectivity between anatomically unconnected areas is shaped by collective network-level effects in the macaque cortex. Cereb Cortex. 2012; 22(7):1586–1592. doi:10.1093/cercor/bhr234. [PubMed: 21893683]

Birn RM, Diamond JB, Smith MA, Bandettini PA. Separating respiratory-variation-related fluctuations from neuronal-activity-related fluctuations in fMRI. Neuroimage. 2006; 31(4):1536–1548. doi: 10.1016/j.neuroimage.2006.02.048. [PubMed: 16632379]

Biswal B, Yetkin FZ, Haughton VM, Hyde JS. Functional connectivity in the motor cortex of resting human brain using echo-planar MRI. Magn Reson Med. 1995; 34(4):537–541. [PubMed: 8524021]

Biswal BB, Van Kylen J, Hyde JS. Simultaneous assessment of flow and BOLD signals in resting-state functional connectivity maps. NMR Biomed. 1997; 10(4–5):165–170. [PubMed: 9430343]

Chen W, Kato T, Zhu XH, Strupp J, Ogawa S, Ugurbil K. Mapping of lateral geniculate nucleus activation during visual stimulation in human brain using fMRI. Magn Reson Med. 1998; 39(1):89–96. [PubMed: 9438442]

Clarke S, Miklossy J. Occipital cortex in man: organization of callosal connections, related myelo- and cytoarchitecture, and putative boundaries of functional visual areas. J Comp Neurol. 1990; 298(2): 188–214. doi:10.1002/cne.902980205. [PubMed: 2212102]

Cordes D, Haughton VM, Arfanakis K, Wendt GJ, Turski PA, Moritz CH, Quigley MA, Meyerand ME. Mapping functionally related regions of brain with functional connectivity MR imaging. AJNR Am J Neuroradiol. 2000; 21(9):1636–1644. [PubMed: 11039342]

Damoiseaux JS, Greicius MD. Greater than the sum of its parts: a review of studies combining structural connectivity and resting-state functional connectivity. Brain Struct Funct. 2009; 213(6): 525–533. doi:10.1007/s00429-009-0208-6. [PubMed: 19565262]

de Zwart JA, Silva AC, van Gelderen P, Kellman P, Fukunaga M, Chu R, Koretsky AP, Frank JA, Duyn JH. Temporal dynamics of the BOLD fMRI impulse response. Neuroimage. 2005; 24(3):667–677. doi:10.1016/j.neuroimage.2004.09.013. [PubMed: 15652302]

de Zwart JA, van Gelderen P, Jansma JM, Fukunaga M, Bianciardi M, Duyn JH. Hemodynamic nonlinearities affect BOLD fMRI response timing and amplitude. Neuroimage. 2009; 47(4):1649–1658. doi:10.1016/j.neuroimage.2009.06.001. [PubMed: 19520175]

de Zwart, JA.; van Gelderen, P.; Duyn, JH. A Case for Correcting Attenuation of Correlation in Resting State fMRI. International Society for Magnetic Resonance in Medicine 21st Annual Meeting & Exhibition; Salt Lake City, UT, USA. Apr 20–26. 2013 p. 2248

Drew PJ, Duyn JH, Golanov E, Kleinfeld D. Finding coherence in spontaneous oscillations. Nat Neurosci. 2008; 11(9):991–993. doi: 10.1038/nn0908-991. [PubMed: 18725901]

Duvernoy, HM. The human brain—Surface, blood supply, and three-dimensional sectional anatomy. 2nd. Springer; Wien New York: 1999.

Glover GH, Li TQ, Ress D. Image-based method for retrospective correction of physiological motion effects in fMRI: RETROICOR. Magn Reson Med. 2000; 44(1):162–167. [PubMed: 10893535]

Honey CJ, Sporns O, Cammoun L, Gigandet X, Thiran JP, Meuli R, Hagmann P. Predicting human resting-state functional connectivity from structural connectivity. Proc Natl Acad Sci USA. 2009; 106(6):2035–2040. doi:10.1073/pnas.0811168106. [PubMed: 19188601]

Johnston JM, Vaishnavi SN, Smyth MD, Zhang D, He BJ, Zempel JM, Shimony JS, Snyder AZ, Raichle ME. Loss of resting interhemispheric functional connectivity after complete section of the corpus callosum. J Neurosci. 2008; 28(25):6453–6458. doi: 10.1523/JNEUROSCI.0573-08.2008. [PubMed: 18562616]

Lowe MJ, Mock BJ, Sorenson JA. Functional connectivity in single and multislice echoplanar imaging using resting-state fluctuations. Neuroimage. 1998; 7(2):119–132. doi:10.1006/nimg.1997.0315. [PubMed: 9558644]

Lu J, Liu H, Zhang M, Wang D, Cao Y, Ma Q, Rong D, Wang X, Buckner RL, Li K. Focal pontine lesions provide evidence that intrinsic functional connectivity reflects polysynaptic anatomical pathways. J Neurosci. 2011; 31(42):15065–15071. doi:10.1523/JNEUROSCI.2364-11.2011. [PubMed: 22016540]

Maier A, Adams GK, Aura C, Leopold DA. Distinct superficial and deep laminar domains of activity in the visual cortex during rest and stimulation. Front Syst Neurosci 4. 2010 doi:10.3389/fnsys. 2010.00031.

Mohajerani MH, McVea DA, Fingas M, Murphy TH. Mirrored bilateral slow-wave cortical activity within local circuits revealed by fast bihemispheric voltage-sensitive dye imaging in anesthetized and awake mice. J Neurosci. 2010; 30(10):3745–3751. doi:10.1523/JNEUROSCI.6437-09.2010. [PubMed: 20220008]

Morel, A. Stereotactic atlas of the human thalamus and basal ganglia. Informa Healthcare USA, Inc.; New York: 2007.

Moruzzi G, Magoun HW. Brain stem reticular formation and activation of the EEG. Electroencephalogr Clin Neurophysiol. 1949; 1(4):455–473. [PubMed: 18421835]

Polimeni JR, Fischl B, Greve DN, Wald LL. Laminar analysis of 7T BOLD using an imposed spatial activation pattern in human V1. Neuroimage. 2010; 52(4):1334–1346. doi:10.1016/j.neuroimage.2010.05.005. [PubMed: 20460157]

Pruessmann KP, Weiger M, Scheidegger MB, Boesiger P. SENSE: sensitivity encoding for fast MRI. Magn Reson Med. 1999; 42(5):952–962. [PubMed: 10542355]

Quigley M, Cordes D, Turski P, Moritz C, Haughton V, Seth R, Meyerand ME. Role of the corpus callosum in functional connectivity. AJNR Am J Neuroradiol. 2003; 24(2):208–212. [PubMed: 12591635]

Rykhlevskaia E, Gratton G, Fabiani M. Combining structural and functional neuroimaging data for studying brain connectivity: a review. Psychophysiology. 2008; 45(2):173–187. doi:10.1111/j.1469-8986.2007.00621.x. [PubMed: 17995910]

Saalmann YB, Kastner S. Gain control in the visual thalamus during perception and cognition. Curr Opin Neurobiol. 2009; 19(4):408–414. doi:10.1016/j.conb.2009.05.007. [PubMed: 19556121]

Saalmann YB, Kastner S. Cognitive and perceptual functions of the visual thalamus. Neuron. 2011; 71(2):209–223. doi:10.1016/j.neuron.2011.06.027. [PubMed: 21791281]

Salvador R, Suckling J, Coleman MR, Pickard JD, Menon D, Bullmore E. Neurophysiological architecture of functional magnetic resonance images of human brain. Cereb Cortex. 2005; 15(9):1332–1342. doi:10.1093/cercor/bhi016. [PubMed: 15635061]

Schneider KA, Kastner S. Visual responses of the human superior colliculus: a high-resolution functional magnetic resonance imaging study. J Neurophysiol. 2005; 94(4):2491–2503. doi:10.1152/jn.00288.2005. [PubMed: 15944234]

Sherman, SM.; Guillery, RW. Exploring the thalamus and its role in cortical function. 2nd. The MIT press; Cambridge: 2006.

Sherman SM, Guillery RW. Distinct functions for direct and transthalamic corticocortical connections. J Neurophysiol. 2011; 106(3):1068–1077. doi:10.1152/jn.00429.2011. [PubMed: 21676936]

Shmueli K, van Gelderen P, de Zwart JA, Horovitz SG, Fukunaga M, Jansma JM, Duyn JH. Low-frequency fluctuations in the cardiac rate as a source of variance in the resting-state fMRI BOLD signal. Neuroimage. 2007; 38(2):306–320. doi:10.1016/j.neuroimage.2007.07.037. [PubMed: 17869543]

Spearman C. The proof and measurement of association between two things. Am J Psychol. 1904; 15:72–101. doi:10.2307/1412159.

Theyel BB, Llano DA, Sherman SM. The corticothalamocortical circuit drives higher-order cortex in the mouse. Nat Neurosci. 2010; 13(1):84–88. doi:10.1038/nn.2449. [PubMed: 19966840]

Tyszka JM, Kennedy DP, Adolphs R, Paul LK. Intact bilateral resting-state networks in the absence of the corpus callosum. J Neurosci. 2011; 31(42):15154–15162. doi:10.1523/JNEUROSCI.1453-11.2011. [PubMed: 22016549]

Uddin LQ, Mooshagian E, Zaidel E, Scheres A, Margulies DS, Kelly AM, Shehzad Z, Adelstein JS, Castellanos FX, Biswal BB, Milham MP. Residual functional connectivity in the split-brain revealed with resting-state functional MRI. NeuroReport. 2008; 19(7):703–709. doi:10.1097/WNR.0b013e3282fb8203. [PubMed: 18418243]

Van Essen DC, Newsome WT, Bixby JL. The pattern of interhemispheric connections and its relationship to extrastriate visual areas in the macaque monkey. J Neurosci. 1982; 2(3):265–283. [PubMed: 7062108]

Whittaker, J. Graphical models in applied multivariate statistics. 1st. Vol. 1. Wiley; New York: 1990.

Worgotter F, Eyding D, Macklis JD, Funke K. The influence of the corticothalamic projection on responses in thalamus and cortex. Philos Trans R Soc Lond B. 2002; 357(1428):1823–1834. doi:10.1098/rstb.2002.1159. [PubMed: 12626015]

Zhang D, Snyder AZ, Fox MD, Sansbury MW, Shimony JS, Raichle ME. Intrinsic functional relations between human cerebral cortex and thalamus. J Neurophysiol. 2008; 100(4):1740–1748. doi:10.1152/jn.90463.2008. [PubMed: 18701759]

Zou Q, Long X, Zuo X, Yan C, Zhu C, Yang Y, Liu D, He Y, Zang Y. Functional connectivity between the thalamus and visual cortex under eyes closed and eyes open conditions: a resting-state fMRI study. Hum Brain Mapp. 2009; 30(9):3066–3078. doi:10.1002/hbm.20728. [PubMed: 19172624]

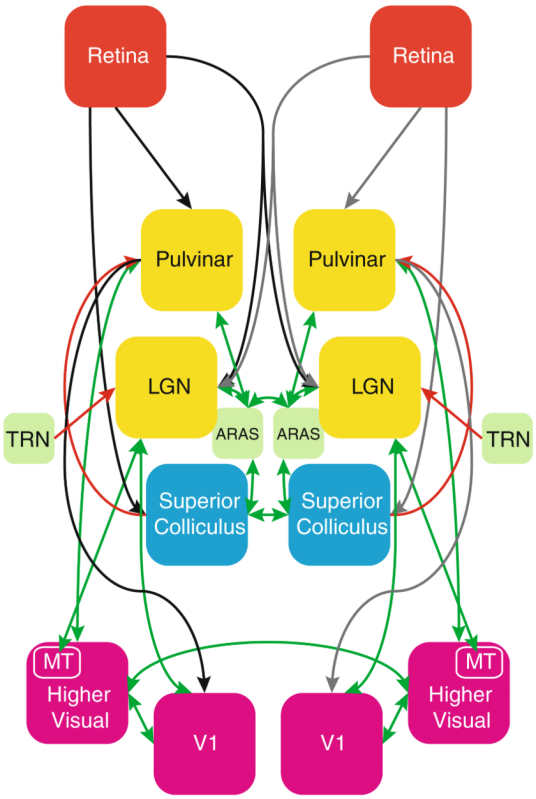

Fig. 1.

Schematic overview summarizing the various brain regions involved in human vision and the pathways connecting them. Forward connections are shown in *black/grey*, feedback connections in *red*, and connections between regions interconnected by both forward and feedback afferents are shown in *green*. (*Arrow-heads* further indicate the direction of each connection.) Acronyms were used for *LGN* lateral geniculate nucleus, *TRN* thalamic reticular nucleus, *ARAS* ascending reticular activating system, *V1* primary visual cortex, *MT* middle-temporal visual area 5. This figure is based on pathways described in literature, see “Introduction” section for more details (Color figure online)

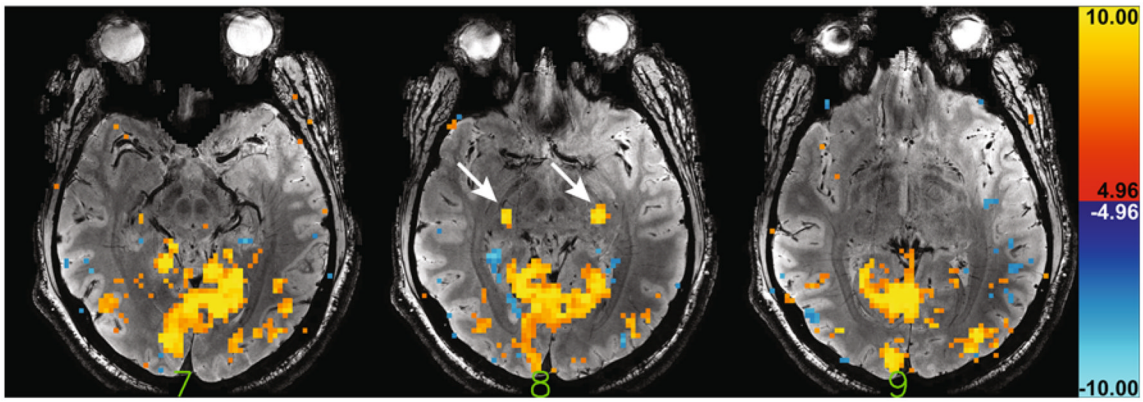

Fig. 2.

Example activation map for the 5-min block paradigm for three slices of one of the volunteers. *Arrows* highlight the distinct bilateral LGN activation in the central of these three slices. A significance threshold of t = 4.96 ($p < 0.05$, corrected for multiple comparisons) was used for the activation overlay. The first echo of the high resolution anatomical data (with 15 ms echo time) for those same three slices, which were used for LGN identification, was used as the underlay

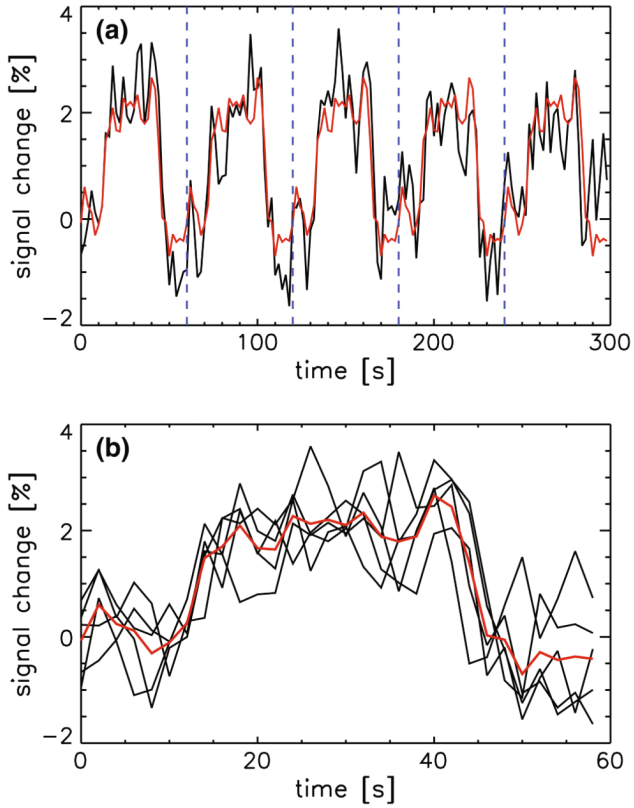

Fig. 3.

The average signal in the visual cortex of one of the volunteers during presentation of the visual task is shown (*black trace* in **a**). Data were split (at *dotted vertical blue lines in* **a**) in the five individual task block periods (*black traces* in **b**), and averaged (*red trace* in **b**). This average signal was subsequently repeated 5 times to yield a regressor for the average response to the block paradigm stimulus (*red trace* in **a**), which is referred to as the *avgresp* regressor in the main text and Table 1 (Color figure online)

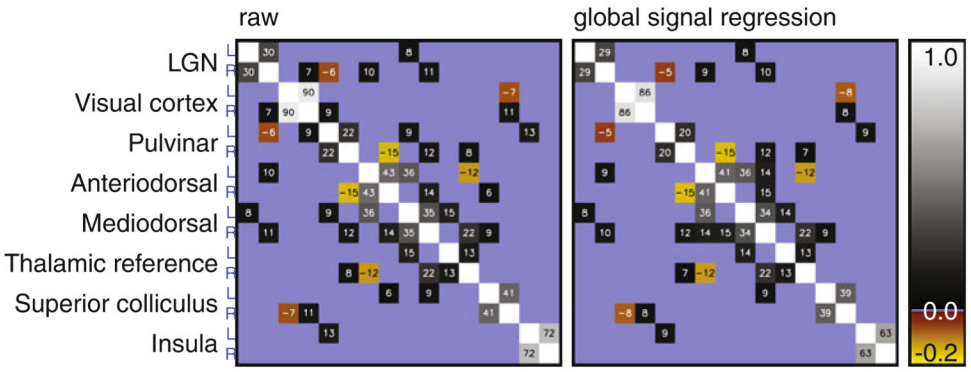

Fig. 4.

Partial correlation matrices for the regions investigated here. ROI-averaged signal from each hemisphere was analyzed separately. The analysis was performed on ROI-averaged time course signals from data not subject to (*left*) and subject to (*right*) global signal regression. Partial correlation was not significant (determined using the variance over volunteers) in areas shaded in *blue*. Values in the other, significantly non-zero, areas are the partial correlation value for that pair or regions multiplied by 100

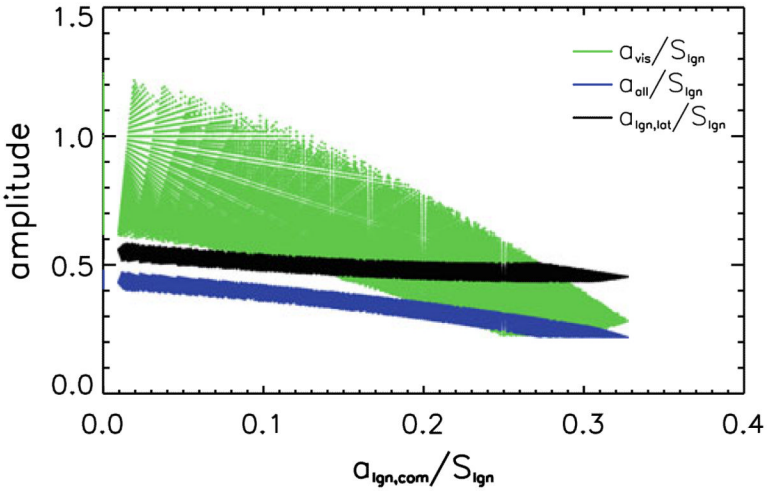

Fig. 5.

Plot of the various source signal amplitudes for sets of Monte Carlo simulation results that are in agreement with experimental findings. The signal component amplitudes (a_{all}, a_{vis} and $a_{lgn,lat}$) for all valid simulated conditions are plotted as a function of $a_{lgn,com}$, the amplitude of a bilateral LGN signal not present in visual cortex. Since the absolute amplitudes (*a*) of the simulated components is not relevant, but merely their relative contribution to the signal in a given area, all amplitudes are scaled to the overall amplitude of the simulated signal in LGN (S_{lgn}), to which several components contribute. (See text for details.)

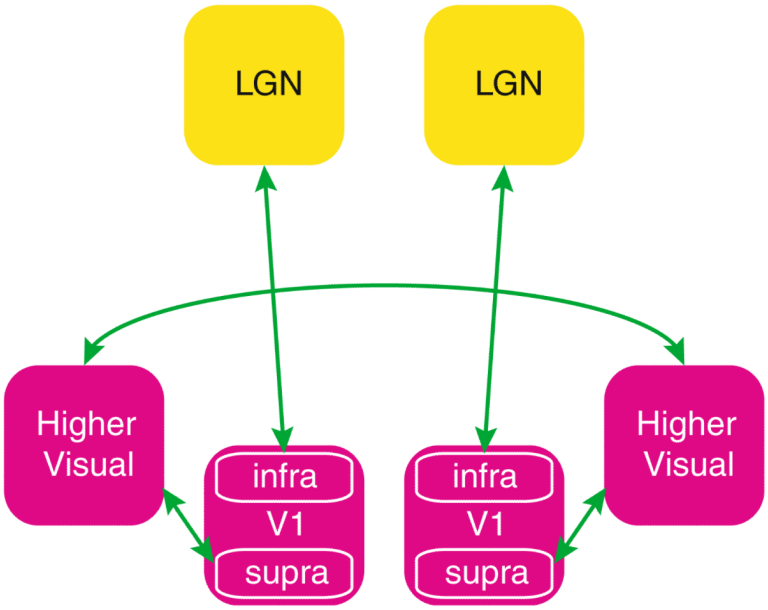

Fig. 6.

Schematic drawing of the connections needed to explain our experimental findings during rest in light of a recent findings by Maier et al. (2010), where correlation in supra-granular layers (‘supra’) shows a strong cortico-cortical connectivity with the other hemisphere, whereas a distinct pattern in infra-granular layers (‘infra’) correlates with LGN, where a lateralized local fluctuation also exists

Table 1

Inter-regional cross correlation values and standard error over volunteers ($n = 8$), where the value for CC(LGN, VIS) is the mean of CC(LGN_L, VIS_L) and CC(LGN_R, VIS_R) and $VIS_{avgresp}$ and $LGN_{avgresp}$ are the mean responses in the visual cortex and LGN over the 5 task blocks, respectively (see text and Fig. 3 for more details)

State	Regressed out	Cross correlation (standard error)		
		CC(LGN_L, LGN_R)	CC(LGN, VIS)	CC(VIS_L, VIS_R)
EC rest	–	0.39 (0.07)	0.29 (0.07)	0.95 (0.01)
	VIS (from LGN)	0.35 (0.06)	–	–
	LGN (from VIS)	–	–	0.85 (0.03)
Task	–	0.67 (0.07)	0.72 (0.04)	0.98 (0.00)
	VIS (from LGN)	0.36 (0.08)	–	–
	LGN (from VIS)	–	–	0.65 (0.03)
	Paradigm (from all)	0.50 (0.07)	0.50 (0.05)	0.96 (0.00)
	$VIS_{avgresp}$ (from LGN)	0.49 (0.08)	0.25 (0.03)	–
	$LGN_{avgresp}$ (from VIS)	–	0.28 (0.03)	0.83 (0.03)

The significance thresholds ($p < 0.05$) for the reported correlation values are 0.17 and 0.21 without and with a correction for multiple (8) comparisons, respectively

Table 2

Intrinsic (image) noise level and mean fluctuation levels, computed as the standard deviation over time during eyes-closed rest, as a percentage of baseline signal for the various regions investigated, both before and after global signal regression

ROI	Intrinsic noise (%)	Fluctuation level over time (%)			
		Voxel level		ROI averaged	
		No GSR	GSR	No GSR	GSR
LGN	0.61 (0.03)	1.56 (0.09)	1.51 (0.08)	0.87 (0.06)	0.83 (0.07)
Visual cortex	0.96 (0.24)	3.34 (0.45)	3.08 (0.42)	1.07 (0.15)	0.67 (0.09)
Thalamic reference	1.07 (0.24)	2.95 (0.48)	2.88 (0.48)	0.71 (0.03)	0.64 (0.02)
Insula	0.38 (0.02)	2.06 (0.18)	1.80 (0.14)	1.19 (0.11)	0.78 (0.08)
Pulvinar	0.59 (0.02)	1.51 (0.13)	1.44 (0.12)	0.56 (0.05)	0.46 (0.03)
Anterodorsal nucleus	0.75 (0.06)	2.83 (0.41)	2.73 (0.40)	1.01 (0.15)	0.91 (0.14)
Mediodorsal nucleus	0.63 (0.03)	2.08 (0.18)	2.00 (0.18)	0.92 (0.06)	0.82 (0.07)
Superior colliculus	0.88 (0.08)	5.22 (0.66)	5.01 (0.61)	1.51 (0.14)	1.31 (0.12)

Values between parentheses are the standard error over volunteers

Table 3

Inter-regional cross correlation values with their standard error over volunteers ($n = 8$), showing the cross correlation of the various regions with LGN and visual cortex, both with and without global signal regression

Global signal regression	SIG	Cross correlation (standard error over volunteers)		
		$CC(SIG_L, SIG_R)$	CC(SIG, LGN)	CC(SIG, VIS)
No	LGN	0.39 (0.07)	–	0.29 (0.07)
	Visual cortex	0.95 (0.01)	0.29 (0.07)	–
	Thalamic reference	0.30 (0.07)	0.16 (0.06)	0.12 (0.07)
	Insula	0.82 (0.03)	0.09 (0.08)	0.47 (0.06)
	Pulvinar	0.42 (0.05)	0.23 (0.06)	0.37 (0.03)
	Anterodorsal nucleus	0.58 (0.10)	0.14 (0.04)	0.14 (0.10)
	Mediodorsal nucleus	0.65 (0.07)	0.31 (0.05)	0.20 (0.08)
	Superior colliculus	0.49 (0.04)	0.13 (0.07)	0.23 (0.10)
Yes	LGN	0.39 (0.06)	–	0.20 (0.06)
	Visual cortex	0.87 (0.03)	0.20 (0.06)	–
	Thalamic reference	0.22 (0.09)	0.12 (0.05)	−0.15 (0.05)
	Insula	0.63 (0.09)	−0.08 (0.06)	−0.08 (0.06)
	Pulvinar	0.27 (0.06)	0.14 (0.06)	0.17 (0.05)
	Anterodorsal nucleus	0.51 (0.12)	0.09 (0.05)	−0.14 (0.09)
	Mediodorsal nucleus	0.57 (0.09)	0.26 (0.04)	−0.12 (0.07)
	Superior colliculus	0.38 (0.07)	0.07 (0.05)	−0.03 (0.05)

The significance thresholds ($p < 0.05$) for the reported correlation values are 0.17 and 0.21 without and with a correction for multiple (8) comparisons, respectively